Original Article

Institution of MECHANICAL ENGINEERS
Journal of MECHANICAL ENGINEERING SCIENCE

Proc IMechE Part C:
J Mechanical Engineering Science
227(2) 276–287

DOI: 10.1177/0954406212449550
pic.sagepub.com
SAGE

Modelling and simulation of gear synchronisation and shifting in dual-clutch transmission equipped powertrains

Paul David Walker[1], Nong Zhang[1], Wenzhang Zhan[2] and Bo Zhu[3]

Abstract

Dual-clutch transmissions have increased in prevalence through the combination of high efficiency and shift quality. This is achieved through the automation of conventional manual transmission synchronisers for gear selection with automated clutch-to-clutch shift control, minimising loss of traction to the road. This article derives a suitably detailed model of a dual-clutch transmission equipped powertrain for the transient simulation and analysis of combined synchroniser engagement and gear shifts. Models are derived for a powertrain equipped with a wet dual-clutch transmission with particular focus on a detailed synchroniser mechanism model, including speed synchronisation, ring unblocking and indexing stages of engagement. To demonstrate the combination of synchroniser engagement with clutch-to-clutch shifting, several simulations are conducted to study the variation of chamfer alignment, vehicle speed and synchroniser engagement timing on powertrain response. Results indicate that vehicle speed and chamfer alignment have only limited impact on the quality of shifting. Synchroniser timing can have a more significant influence on shift quality, stressing the need for independence of these processes.

Keywords

Dual-clutch transmission, synchroniser, shift transient, powertrain, dynamics

Date received: 30 October 2011; accepted: 2 May 2012

Introduction

Dual-clutch transmissions (DCTs) combine manual transmission gears and synchronisers with automatic transmission clutch control to provide high-quality shift characteristics with no loss of traction load to the road. Gear change is achieved through the engagement of synchronisers to select the desired ratio before shifting between the two clutch packs. The purpose of this article is to study the powertrain response to the entire shift process, including synchroniser engagement and clutch-to-clutch gear change. To achieve this objective, a comprehensive model of a vehicle powertrain equipped with a DCT is presented which integrating both these components of gear shift.

Shift-control strategies for DCTs are well defined in a range of current research, such as Goetz,[1] Kulkarni et al.,[2] Liu et al.[3] and Goetz et al.,[4–6] where clutch speed and torque are used as references to manipulate input pressure to the clutches. Shifting is realised by reducing engaged clutch pressure and increasing target clutch pressure while minimising undesirable transient vibrations, vehicle surging and the loss of tractive load to the road. Additionally, both vehicle speed and output torque are commonly used to demonstrate shift quality. In a most comprehensive study of up-shift, down-shift and skip-shift control strategies for DCTs, Goetz et al.[1,4–6] present a range of control algorithms with integrated engine and clutch control, including separate strategies for torque and inertia phase of gear shift. Alternative control strategies such as fuzzy logic

[1]School of Electrical, Mechanical and Mechatronic Systems, University of Technology, Sydney, Australia
[2]Advanced Technologies Research Department, Beijing Automotive Technology Centre, Beijing, China
[3]Beijing Electric Vehicles, Beijing, China

Corresponding author:
Paul Walker, School of Electrical, Mechanical and Mechatronic Systems, University of Technology, Sydney, PO Box 123, Broadway, NSW 2007, Australia
Email: Paul.Walker@uts.edu.au

based control have been adopted in Xuexun et al.[7] and Cheng and Wang,[8] with low-order powertrain models, making use of measures such as vehicle jerk to evaluate shift quality. Application of torque rate limitation combined with coupling of primary clutch controllers in Kim et al.[9] was successfully used for gear-shift control. However, there was a significant torque hole present during the transition between torque and inertia phases of shifting. In Walker et al.,[10] independent clutch control was used to demonstrate the minimisation of this torque hole. Additionally, torque overlap and precision of clutch pressure control were both demonstrated to have an impact on shift quality.

High-quality shift control is critical to minimising transient vibration of DCT-equipped powertrains, and while synchroniser engagement is not considered to be an issue for gear-shift control, its actuation is a precursor to shifting, and successful engagement is necessary. Consequently, investigation of synchroniser engagement should be studied in conjunction with clutch-to-clutch shifting. Current consideration of synchroniser engagement is focused on requirements with control applications, where Goetz,[1] Kulkarni et al.[2] and Galvagno et al.[11] model the speed synchronisation phase of synchronisation alone, with the cone clutch torque as a function of friction and slip speed. These do not consider ring unblocking and indexing stages in synchroniser engagement, both of which are critical to the engagement process.

According to Liu and Tseng,[12] Hoshino[13] and Walker and Zhang,[14] the main considerations for synchroniser engagement are (a) speed synchronisation, where the gear speed is matched to the shaft through application of a cone clutch; (b) ring unblocking, where the ring and cone clutch are returned to the neutral position to allow the sleeve to engage target gear; and (c) indexing, where the sleeve locks the target gear to the shaft via chamfered splines to allow the transmission of torque between the shaft and the gear. Research by Liu and Tseng[12] and Hoshino[13] for manual transmissions and Walker and Zhang[14] for DCTs, all demonstrate that a significant portion of the engagement time for synchronisers is taken up ring unblocking and indexing in addition to speed synchronisation. The actuation of the synchroniser produces highly nonlinear torque output, and the duration of engagement is highly dependent on the alignment during the final indexing stage;[12] here, inconsistent alignment in hub and sleeve dog gear at the beginning of indexing contributes to a significant variation in engagement time. Socin and Walters[15] provide a comprehensive discussion of synchroniser mechanisms, indicating block out, or hard shifting, is a result of drag torque exceeding either cone clutch torque or blocking chamfer torque. Whilst clash of sleeve and chamfer can result if cone clutch torque is too low, it frequently occurs if oil wiping fails. Thus, studying synchroniser engagement should consider each step of the engagement process. In this article, a model of the synchroniser that is representative of the complete actuation process will be developed to evaluate its response during engagement and how it impacts on shift dynamics in the DCT.

The characteristics of synchroniser engagement and the impact that this may have on shifting are not studied in detail within the framework of DCT-equipped powertrains. Consequently, this article will investigate shift dynamics of such a powertrain, including the detailed synchroniser mechanism engagement. To achieve this, the remainder of this article is divided into the following components. Following is the presentation of a 'powertrain' model, including clutch and synchroniser torque modelling. The process for synchroniser and shift control is then detailed in 'Transmission control'. Next, 'Simulations' are conducted, studying both synchroniser engagement and gear shift, with variation of synchroniser alignment, vehicle speed and shift timing. Finally, 'concluding' remarks are made.

Modelling of a DCT powertrain with synchronisers

Powertrain

Gear shift in DCTs is realised through the engagement of different combination of synchronisers and clutches to transmit engine torque to the wheels. As a consequence, the rotational inertia and degrees of freedom (DOFs) of the powertrain will change as different clutches and synchronisers are engaged. These changes in inertia can be used to define powertrain states. Consider a third- to fourth-gear up-shift as an example. The different states can then be defined thus:

State 1: Before and during synchronisation, third gear is engaged and clutch 1 (CL1) is closed in transmission, whilst the other gears and synchronisers are open. According to the model presented, there are 13 rotational DOFs.

State 2: After synchronisation is complete, the fourth gear is locked to the output shaft and a DOF is lost as synchroniser sleeve and gear inertias combine, reducing the DOF to 12.

State 3: During shifting, CL1 opens and separation of drum and clutch plates increase the inertia elements by one, and with clutch 2 (CL2) energised, but slipping, the DOF increases to 13.

State 4: Post gear shift, CL2 locks with the drum; the shift process completes and the DOF reduces to 12 with CL1 open.

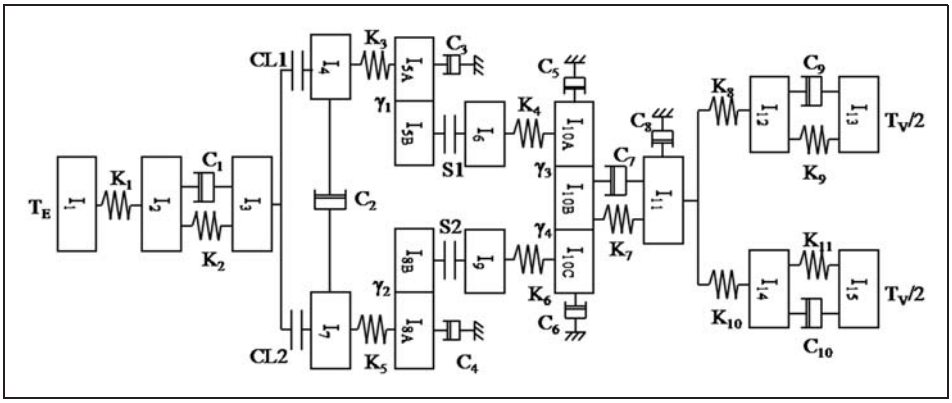

Figure 1. Powertrain model layout for a DCT with synchroniser mechanism.
DCT: dual-clutch transmission.

To capture the shift characteristics of the system, the powertrain is modelled using torsional lumped parameters. Inertia elements represent the major components of the powertrain, such as engine, clutch drum, gears and synchronisers, differential, and wheel and vehicle inertias. Whereas torsional shaft stiffness represents spring elements connecting major components, losses are represented as damping elements. This model is presented in Figure 1, with transmission ratios indicated by $\gamma_1 - \gamma_4$ for third, fourth and the two final drive ratios, respectively (see Table 2 in Appendix 2). The powertrain is structured such that the first three elements represent engine, flywheel and clutch drum. Two coupled clutches, CL1 and CL2, split the transmission into parallel gear sets, enabling clutch-to-clutch shifting. Each set contains clutch plates, reduction gear pair and synchroniser, denoted as S1 and S2. The transmission then has two separate inputs to the final drive, which outputs to parallel wheel hubs and vehicle inertia elements.

The powertrain model equations of motion are derived through application of Newton's second law of motion. In doing so, it is assumed that viscous drag in the wet clutch can be represented as coupled damping between the two clutch packs and idling gears can be lumped as additional inertia on gears targeted for shifting. Backlash in gears is ignored as frequencies excited in lash are generally significantly higher than the main powertrain natural frequencies of 3–100 Hz and are unlikely to impact on synchroniser engagement. De la Cruz[16] demonstrates that backlash frequencies are above 1000 Hz.

First consider State 1, here CL1 and synchroniser one (S1) are both closed, whilst CL2 and synchroniser two (S2) are both open. The model equations of motion are

$$I_1\ddot{\theta}_1 = T_E - K_1(\theta_1 - \theta_2) \tag{1}$$

$$I_2\ddot{\theta}_2 = K_1(\theta_1 - \theta_2) - K_2(\theta_2 - \theta_3) - C_1\left(\dot{\theta}_2 - \dot{\theta}_3\right) \tag{2}$$

$$\begin{aligned}(I_3 + I_4)\ddot{\theta}_3 = {} & K_2(\theta_2 - \theta_3) + C_1\left(\dot{\theta}_2 - \dot{\theta}_3\right) - K_3(\theta_3 - \theta_{5A}) \\ & - C_2\left(\dot{\theta}_3 - \dot{\theta}_7\right) - T_{C_2}\end{aligned} \tag{3}$$

$$\begin{aligned}\left(I_{5A} + (I_{5B} + I_6)/\gamma_1^2\right)\ddot{\theta}_{5A} = {} & K_3(\theta_3 - \theta_{5A}) \\ & - K_4/\gamma_1(\theta_{5A}/\gamma_1 - \gamma_3\theta_{10B}) - C_3\dot{\theta}_{5A}\end{aligned} \tag{4}$$

$$I_7\ddot{\theta}_7 = T_{C_2} - K_5(\theta_7 - \theta_{8A}) + C_2\left(\dot{\theta}_3 - \dot{\theta}_7\right) \tag{5}$$

$$\left(I_{8A} + I_{8B}/\gamma_2^2\right)\ddot{\theta}_{8A} = K_5(\theta_7 - \theta_{8A}) - T_{S2}/\gamma_2 - C_4\dot{\theta}_{8A} \tag{6}$$

$$I_9\ddot{\theta}_9 = T_{S2} - K_6(\theta_9 - \gamma_4\theta_{10B}) \tag{7}$$

$$\begin{aligned}\left(I_{10B} + \gamma_3^2 I_{10A} + \gamma_4^2 I_{10C}\right)\ddot{\theta}_{10B} = {} & \gamma_4 K_6(\theta_9 - \gamma_4\theta_{10B}) \\ & + \gamma_3 K_4(\theta_{5A}/\gamma_1 - \gamma_3\theta_{10B}) - (\gamma_3 C_5 + \gamma_4 C_6)\dot{\theta}_{10B} \\ & - K_7(\theta_{10B} - \theta_{11}) - C_7\left(\dot{\theta}_{10B} - \dot{\theta}_{11}\right)\end{aligned} \tag{8}$$

$$\begin{aligned}I_{11}\ddot{\theta}_{11} = {} & K_7(\theta_{10B} - \theta_{11}) + C_7\left(\dot{\theta}_{10B} - \dot{\theta}_{11}\right) \\ & - K_8(\theta_{11} - \theta_{12}) - K_{10}(\theta_{11} - \theta_{14})\end{aligned} \tag{9}$$

$$I_{12}\ddot{\theta}_{12} = K_8(\theta_{11} - \theta_{12}) - K_9(\theta_{12} - \theta_{13}) - C_9\left(\dot{\theta}_{12} - \dot{\theta}_{13}\right) \tag{10}$$

$$I_{13}\ddot{\theta}_{13} = K_9(\theta_{12} - \theta_{13}) + C_9\left(\dot{\theta}_{12} - \dot{\theta}_{13}\right) - T_V/2 \quad (11)$$

$$I_{14}\ddot{\theta}_{14} = K_{10}(\theta_{11} - \theta_{14}) - K_{11}(\theta_{14} - \theta_{15}) - C_{10}\left(\dot{\theta}_{14} - \dot{\theta}_{15}\right) \quad (12)$$

$$I_{15}\ddot{\theta}_{15} = K_{11}(\theta_{14} - \theta_{15}) + C_{10}\left(\dot{\theta}_{14} - \dot{\theta}_{15}\right) - T_V/2 \quad (13)$$

In State 2, in addition to CL1 and S1 being closed, S2 is also closed. Equations (6) and (7) and (6) and (8) are replaced with equations (14) and (15).

$$\left(I_{8A} + (I_{8B} + I_9)/\gamma_2^2\right)\ddot{\theta}_{8A} = K_5(\theta_7 - \theta_{8A}) - K_6/\gamma_2(\theta_{8A}/\gamma_2 - \gamma_4\theta_{10B}) - C_4\dot{\theta}_{8A} \quad (14)$$

$$(I_{10B} + \gamma_3^2 I_{10A} + \gamma_4^2 I_{10C})\ddot{\theta}_{10B} = \gamma_4 K_6(\theta_{8A}/\gamma_2 - \gamma_4\theta_{10B}) + \gamma_3 K_4(\theta_{5A}/\gamma_1 - \gamma_3\theta_{10B}) - (\gamma_3 C_5 + \gamma_4 C_6)\dot{\theta}_{10B} - K_7(\theta_{10B} - \theta_{11}) - C_7(\dot{\theta}_{10B} - \dot{\theta}_{11}) \quad (15)$$

During gear shift in State 3, beginning with equations of motion for State 2, equation (3) is expanded to equations (16) and (17).

$$I_3\ddot{\theta}_3 = K_2(\theta_2 - \theta_3) + C_1\left(\dot{\theta}_2 - \dot{\theta}_3\right) - T_{C_1} - T_{C_2} \quad (16)$$

$$I_4\ddot{\theta}_4 = T_{C_1} - K_3(\theta_3 - \theta_{5A}) - C_2\left(\dot{\theta}_4 - \dot{\theta}_7\right) \quad (17)$$

Finally, for State 4, based on equations of motion for State 3, equation (7) is combined with equation (16) for equation (18), and equations (17) and (14) are replaced with equations (19) and (20).

$$(I_3 + I_7)\ddot{\theta}_3 = K_2(\theta_2 - \theta_3) + C_1\left(\dot{\theta}_2 - \dot{\theta}_3\right) - K_5(\theta_3 - \theta_{8A}) + C_2\left(\dot{\theta}_4 - \dot{\theta}_3\right) - T_{C_1} \quad (18)$$

$$I_4\ddot{\theta}_4 = T_{C_1} - K_3(\theta_3 - \theta_{5A}) - C_2\left(\dot{\theta}_4 - \dot{\theta}_3\right) \quad (19)$$

$$\left(I_{8A} + (I_{8B} + I_9)/\gamma_2^2\right)\ddot{\theta}_{8A} = K_5(\theta_3 - \theta_{8A}) - K_6/\gamma_2(\theta_{8A}/\gamma_2 - \gamma_4\theta_{10B}) - C_4\dot{\theta}_{8A} \quad (20)$$

The elements of the powertrain model and respective values are detailed in Table 3 of Appendix 2.

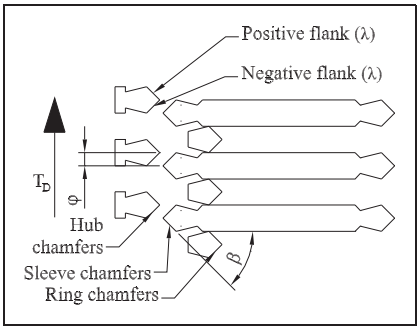

Figure 2. Engine torque map.

Engine and vehicle torques

To reduce the computational demand for simulations, engine torque is modelled using a mean torque look-up table with output torque as a function of speed and percent throttle, see Figure 2. This method excludes the modelling engine torque harmonics from simulations, justifiable as Fredriksson and Karlsson[17] indicates that engine harmonics are unlikely to interact with major powertrain natural frequencies and therefore will not influence shift control.

Vehicle resistance torque is derived from rolling, aerodynamic and incline load, detailed in equation (21).

$$T_V = \left(M_v g \sin(\varphi) + \frac{1}{2}\rho_{air} A_v C_D V^2 + M_v g C_T\right) \times R_W \quad (21)$$

where T_V is vehicle torque, M_V vehicle mass, φ road grade, ρ_{air} air density, A_V frontal area of the vehicle, C_D the drag coefficient, V the linear velocity of the vehicle, C_T the rolling resistance of the tyre and R_W the wheel radius.

Clutch torque

Mean radius for dynamic friction torque in CL1 and CL2 is calculated according to Vasca et al.,[18] where the mean radius of friction surfaces is methodically derived. The significant change when applied to wet clutches is the inclusion of multiple friction surfaces, as indicated by the parameter n. This equation is modified in equation (22) to create a piecewise clutch torque model in a method similar to Crowther et al.,[19] capable of simulating stick-slip in the model as clutches release and lock. As an example, if the transmission is driving through third gear with the corresponding clutch in an open state, viscous friction is modelled according to equations (3) and (5) and there is no dry friction in the

clutch, as signified by line 1 of equation (22). Line 2 of equation (22) indicates contact friction in the clutch when the pack is energised, with lines 2–4 used to simulate the stick-slip friction relationship, see Crowther et al.[19] for details.

$$T_C = \begin{cases} 0 & X < X_0 \\ n\mu_D \frac{2}{3}\frac{r_O^3 - r_I^3}{r_O^2 - r_I^2} \times F_A & X \geqslant X_0, \left|\Delta\dot{\theta}\right| > 0^* \\ T_{avg} & X \geqslant X_0, \left|\Delta\dot{\theta}\right| < 0^*, T_{avg} < T_{C,S} \\ n\mu_S \frac{2}{3}\frac{r_O^3 - r_I^3}{r_O^2 - r_I^2} \times F_A & X \geqslant X_0, \left|\Delta\dot{\theta}\right| < 0^*, T_{avg} \geqslant T_{C,S} \end{cases} \quad (22)$$

where n is the number of friction surfaces, X the piston displacement, X_0 the minimum displacement required for contact between friction plates, μ_D the dynamic friction, μ_S the static friction, r_O and r_I the outside and inside radii of the clutch plates and F_A the force resulting from the hydraulic load on the clutch.

T_{avg} is the average torque in an engaged clutch. For CL2, this is derived from the model dynamics by arranging equations (16) and (7) in terms of T_{C_2}, and the average taken of the two equations, as shown in equations (23) to (25).

$$T_{avg} = \frac{T_{C_{2A}} + T_{C_{2B}}}{2} \quad (23)$$

$$T_{C_{2A}} = K_2(\theta_2 - \theta_3) + C_1\left(\dot{\theta}_2 - \dot{\theta}_3\right) - T_{C_1} - I_3\ddot{\theta}_3 \quad (24)$$

$$T_{C_{2B}} = I_7\ddot{\theta}_7 + K_5(\theta_7 - \theta_{8A}) - C_2\left(\dot{\theta}_4 - \dot{\theta}_7\right) \quad (25)$$

Synchroniser torque

The synchroniser model is adopted from Walker and Zhang[14] where cone, blocking and indexing torques are described. The sleeve is driven by hydraulic actuators, comprising of high-flow on/off solenoids actuating a double-acting piston arrangement; this model is detailed in Walker and Zhang.[14] Cone clutch and indexing torque must be considered in a piecewise manner depending on the state of engagement and load on the mechanism. The piecewise cone torque model is realised through the combination Socin and Walters[15] and Paffoni et al.[20] with stick-slip friction models.[19] Equation (26) combines the viscous friction when the cone clutch is open with a relative velocity. When the cone clutch is energised, dynamic friction torque drives the synchronisation process, see line 2 of equation (26). Once the cone clutch synchronises, the torque changes to the estimated torque from equation (27) and is limited by the static friction coefficient in the cone clutch using a stick-slip algorithm.

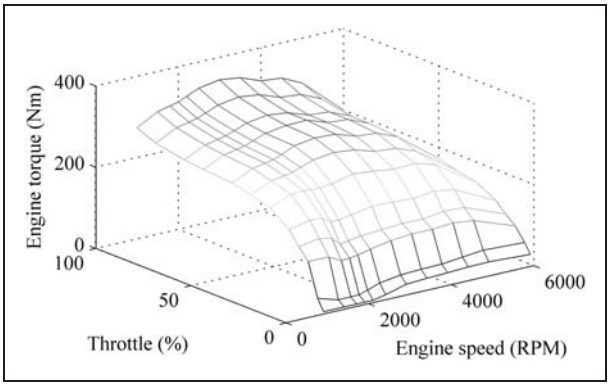

Figure 3. Chamfer alignment conditions for synchroniser mechanism, showing the net resistance torque, T_D, contact flank, λ and relative alignment, φ.

$$T_C = \begin{cases} 4\pi\mu R_C^3 b \frac{\dot{\theta}_{syn}}{h} & X_S < X_{S0},\ \dot{\theta} \neq 0 \\ \frac{f_C F R_C}{\sin\alpha} & X_S \geqslant X_{S0},\ \dot{\theta} \neq 0 \\ T_{SYN} & X_S \geqslant X_{S0},\ \dot{\theta} = 0, T_{SYN} \leqslant T_{C,S} \\ \frac{f_{C,S} F R_C}{\sin\alpha} & X_S \geqslant X_{S0},\ \dot{\theta} = 0, T_{SYN} > T_{C,S} \end{cases} \quad (26)$$

where T_C is the cone torque, $T_{C,S}$ the static friction torque from line 4 of equation (26), X_S the sleeve displacement, X_{S0} the clearance between the sleeve neutral point and contact with ring chamfers, μ the lubricant viscosity, R_C the cone mean radius, b the half-cone generatrix, h the cone separation, f_C the cone friction coefficient, $f_{C,S}$ the static friction, F the sleeve force, α the cone angle and $T_{C,S}$ the static torque in the cone.

Here, T_{SYN} is the average synchroniser torque and is derived from equation (6) thus

$$T_{SYN} = -\gamma_2\left[\left(I_{8B}/\gamma_2^2 + I_{8A}\right)\ddot{\theta}_{G2} + K_5(\theta_{8A} - \theta_7) - C_4\dot{\theta}_{8A}\right] \quad (27)$$

Synchroniser cone slip speed is

$$\dot{\theta}_{SYN} = \gamma_2\dot{\theta}_{5A} - \dot{\theta}_6 \quad (28)$$

This equation is maintained through the speed synchronisation and ring unblocking steps of engagement according to Walker and Zhang.[14]

The blocking, or indexing, torque is dependent on the direction of sleeve velocity ($\dot{x}$) and flank of chamfer engagement (λ), see Figure 3. Derived from the results of Hoshino,[13] a negative sleeve velocity produces friction loss in a positive direction, thus the positive sign in the numerator of equation lines 2 and 4, whilst a negative flank contact produces an overall negative direction of chamfer torque, seen in lines 3 and 4. Indexing torque is represented as

$$T_I = \begin{cases} FR_I \dfrac{1-\mu_I \tan\beta}{\mu_I + \tan\beta} & \lambda + \text{ve}, \dot{x} + \text{ve} \\ FR_I \dfrac{1+\mu_I \tan\beta}{-\mu_I + \tan\beta} & \lambda + \text{ve}, \dot{x} - \text{ve} \\ -FR_I \dfrac{1-\mu_I \tan\beta}{\mu_I + \tan\beta} & \lambda - \text{ve}, \dot{x} + \text{ve} \\ -FR_I \dfrac{1+\mu_I \tan\beta}{-\mu_I + \tan\beta} & \lambda - \text{ve}, \dot{x} - \text{ve} \end{cases} \quad (29)$$

where R_I is the chamfer mean radius, μ_I the chamfer friction coefficient and β the chamfer angle.

The torques defined in equations (28) and (29) represent the different steps of synchroniser engagement, culminating the locking of the target gear to the lay shaft in preparation for shifting. Throughout the entire engagement process, there is a strict reliance on the balancing of torques to ensure that engagement is successful. For example, during speed synchronisation, if the blocking torque exceeds cone clutch torque before the conical clutch is synchronised, the mechanism will unblock prematurely and the sleeve will come in to contact with the target gear while there is a high relative speed between indexing chamfers on sleeve and gear hub, causing audible clash. This is observed as a grinding sound in manual transmissions.[15] Note that the synchroniser parameters corresponding to equations (26) and (29) are presented in Table 1.

Table 1. Synchroniser parameters.

Parameter	Units	Value	Parameter	Units	Value
f_C	–	0.12	μ_I	–	0.04
R_C	mm	47.5	R_I	mm	60
α	°	7	β	°	65

Transmission control

Shift control in DCTs is a sequential process, where the gear targeted for shifting is engaged by the synchroniser prior to the initiation of gear shift. Following gear synchronisation, clutch control proceeds through shift preparation, torque phase, inertia phase and shift completes with locking of the target clutch. Depending on engine speed, the gear engaged in the transmission synchronisation can take from 100 to 400 ms, whilst the complete gear shift can take 400–900 ms, including synchronisation, clutch preparation, toque phase, inertia phase and clutch lock-up. The timing of synchroniser actuation and clutch preparation is important to balance such that there is a minimal delay between the detection of shift command and the completion of gear shift, particularly for driver-override commands.

The synchroniser actuation arrangement and pressures are shown in Figure 4. The double-acting hydraulic cylinder is used to push the sleeve in one of the two directions to engage two different gears. The resulting pressure is reactive in nature as the system response to sleeve displacement such that when sleeve displacement is initiated, as indicated at (a), the pressure drops as the sleeve fills the opening hydraulic cylinder. As the sleeve is released after ring unblocking, pressure reduces at (b) until it comes in contact with the indexing chamfers. The system rapidly pressurises as resistance increases and the engagement process is completed. As with double-acting cylinder arrangements, while the active cylinder rapidly expands the idle cylinder contracts and, as a consequence, the idle cylinder experiences back pressure as fluid is forced from the cylinder.

Clutch-to-clutch shift control makes use of a relatively simple shift strategy; this was presented in Walker et al.[21] Here, shifting is realised through a combination of clutch pressure and engine torque control to minimise the duration of shifting without excessive vehicle acceleration. The primary processes in shift control are highlighted in Figure 5, as:

1. Shift preparation – CL1 pressure is reduced to the point of slip, and CL2 piston is filled with to near contact in friction plates.
2. Torque phase – lasting approximately 50 ms, the torque driving the vehicle is transferred from CL1 to CL2. CL1 pressure is reduced and CL2 pressure increased, while engine throttle is maintained to help reduce the torque hole.
3. Inertia phase – with CL2 driving the powertrain, the slip speed between CL2 and the drum is reduced to zero. This takes approximately 250 ms, and to minimise the duration, engine throttle is reduced to zero.
4. Clutch lock-up – here, CL2 pressure is set to maximum once the slip speed is reduced to zero, indicating the completion of shifting.

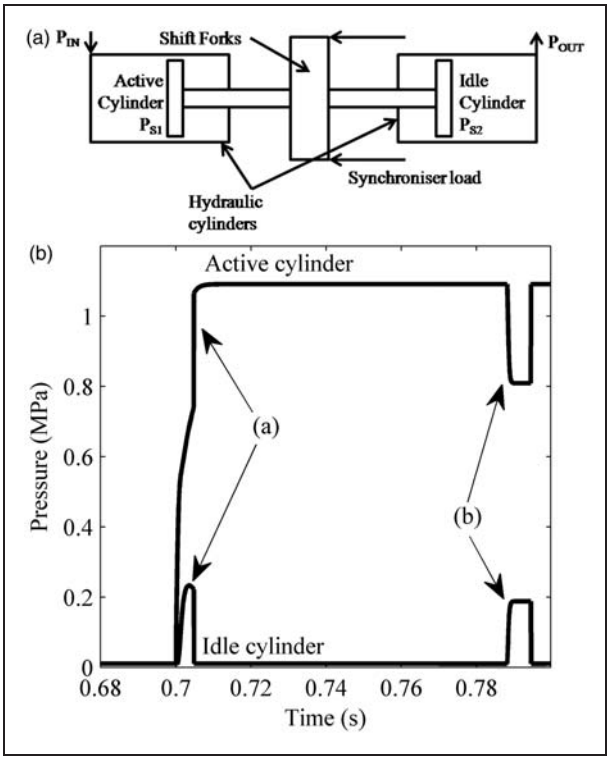

Figure 4. (a) Double-acting cylinder arrangement and (b) synchroniser pressure response during actuation.

Numerical simulations

The powertrain model is constructed in the Matlab environment using the ODE suite using ODE45 with a maximum time step of 10^{-5} s, with event functions used to detect state changes and switch between powertrain model variants as described in 'Powertrain'. For all simulations, the third gear is engaged, and the engine speed is initially 300 rad/s, with an equivalent rotational speed of approximately 68 rad/s at the wheels. Shift transient simulations are conducted for the gear synchronisation of fourth gear, followed by clutch-to-clutch shifting to complete a third-to-fourth gear up-shift.

The combined shift is presented in Figure 6(a), demonstrating speed variation and slip speed variation for the clutches, clutch drum, S2, gear 2, and sleeve 2. The two distinct transient phases are from 0.7 s to approximately 0.8 s; this is gear synchronisation; the second, gear shifting occurs from 1.1 s to approximately 1.35 s. Before synchronisation, clutch and gear 2 speeds are maintained by a combination of the viscous clutch drag, modelled using damping element C_2, and transmission losses, modelled using damping element C_4. The effective torques derived from these terms act to minimise the net torque acting on freewheeling elements I_7 and I_{8A}, as a result the freewheeling speed of these components is higher than the sleeve speed, see Figure 6(a) at 0.6–0.7 s.

Figure 6(b) shows the synchronisation component of shifting alone in detail; each of the main components of synchroniser engagement are indicated. These are (a) steady-state period, (b) speed synchronisation, (c) ring unblocking, (d) second free fly, (e) hub indexing and (f) final steady state. During speed synchronisation at (a), the freewheeling gear is brought to the target speed of the shaft using cone clutch torque. However, as a result of high clutch drag and low cone clutch load at the completion of ring unblocking at (c), the gear enters the second free-fly period without synchronisation of gear and shaft. The relative velocity aids indexing at (e), with an indexing period of less than 10 ms, but creates an impulse at the completion of indexing as dog gears interlock. This clearly results from the trapping of sleeve splines in the hub chamfers while there is still a relative velocity between the mating components, this may be perceived as 'partial clash' type failure as indicated in Socin and Walters.[15]

After gear synchronisation is completed, the shift process is initiated. Pressure is reduced in CL1 according to Figure 5, and CL2 is filled to the point of contact in friction plates. At this time, the torque phase is initiated and there is a drop in CL1 and drum speeds, perceived as a torque hole. Torque phase ends with the initiation of slip in CL1, signifying inertia phase, where clutch drum speed is reduced to CL2 speeds through the application of friction torque in CL2. There is some indication that vibration during the inertia phase is initiated in the torque phase from pull down of CL1 speed. The inertia phase lasts over 200 ms, and on completion, the powertrain vibrates at the main shuffle frequency of 6 Hz.

Influence of chamfer alignment

Research in Liu and Tseng[12] and Hoshino[13] demonstrates that the alignment of chamfers during indexing contributes to variability in synchroniser engagement. The relative alignment between chamfers, φ, is limited to a range of 0 to $2\pi/N_C$, where N_C is the number of chamfers (Figure 3). The following simulation predefines this alignment to produce a negative contact flank engagement at the beginning of indexing; this is an alternative alignment to the positive flank contact in simulations in Figure 6.

The most significant change in engagement is indicated in Figure 7(b). This shows that, at the beginning of indexing, the gear speed is slowed as the negative contact flank produces a torque that opposes the relative speed between sleeve 2 and gear 2. The sleeve displacement demonstrated in Figure 8 shows the impact of this relative motion on synchroniser engagement,

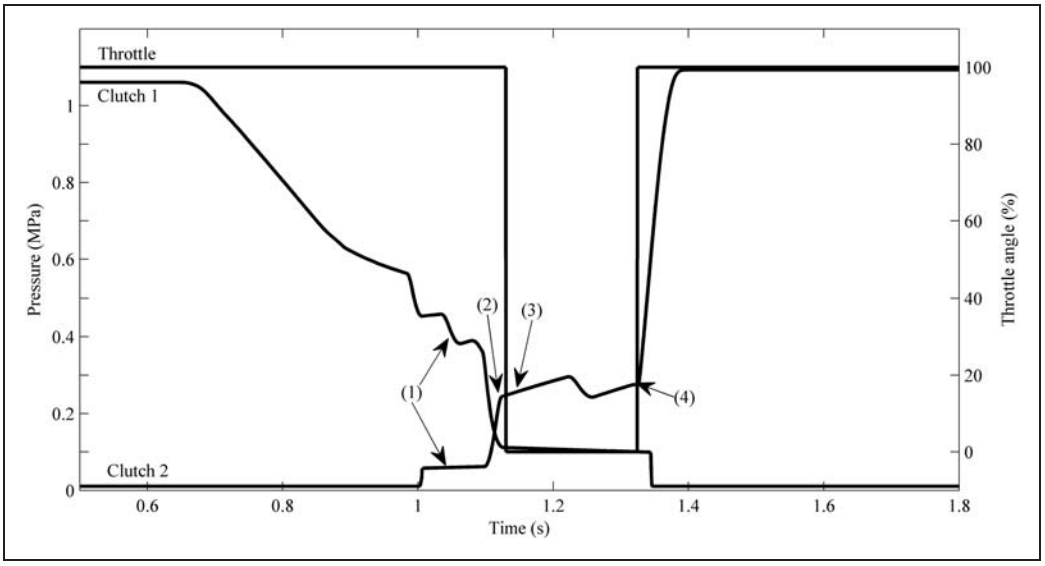

Figure 5. Clutch pressure and engine throttle control signals: (1) shift preparation, (2) torque phase, (3) inertia phase and (4) clutch lock-up.

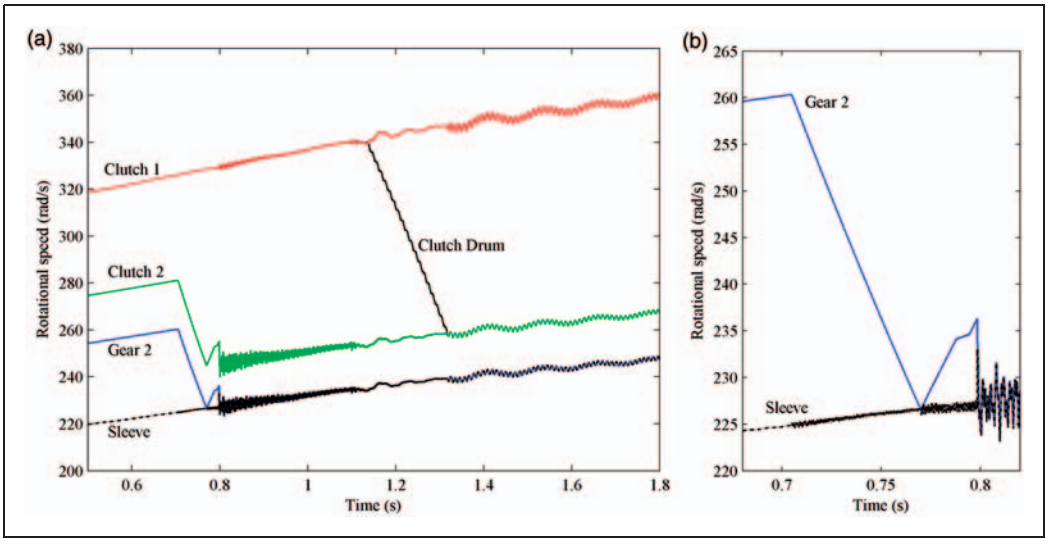

Figure 6. (a) Simulation results for synchroniser engagement and shift transient for complete shift and (b) synchroniser engagement.

where the sleeve is forced backwards in the negative alignment case, as indicated at (b). This is consistent with the results demonstrated in Liu and Tseng[12] and Hoshino,[13] where variation in alignment results in discrepancy in engagement times and sleeve motion. Primarily, this is a result of the relative speed at the end of ring unblocking impinging on chamfer realignment when relative speed and applied torque oppose.

Influence of vehicle speed

The duration of shifting is greatly influenced by the vehicle speed and the gear ratio selected. This is also true for the resistance torque, also referred to as drag torque, which defines the steady-state speed of the synchroniser in relation to vehicle speed. For the proposed model, elements associated with equations (5) and (6) are synchronised. These elements (gear pair 2 and CL2) have torque losses that can be termed as drag torque. From equation (5), drag losses are $C_2(\dot{\theta}_3 - \dot{\theta}_7)$ from relative speed in the open clutch, and from equation (6), losses are defined as $C_4\dot{\theta}_{8A}$, which are losses associated with the gear, such as tooth friction or windage. The speed dependency of these losses will affect the steady-state speed and net resistance on the synchroniser in a nonlinear manner.

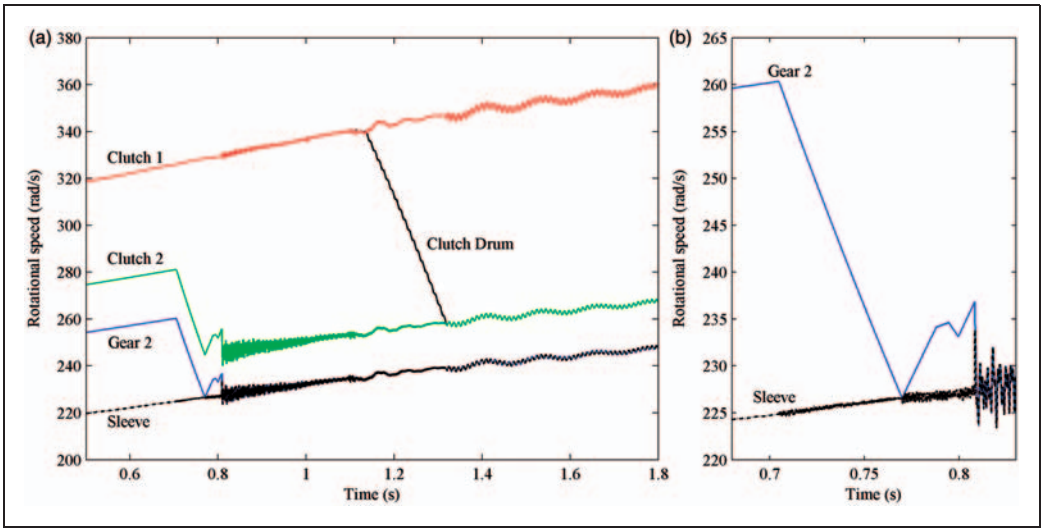

Figure 7. Simulation results for alternative chamfer flank contact (λ): (a) synchroniser engagement and shift transient for complete shift and (b) synchroniser engagement.

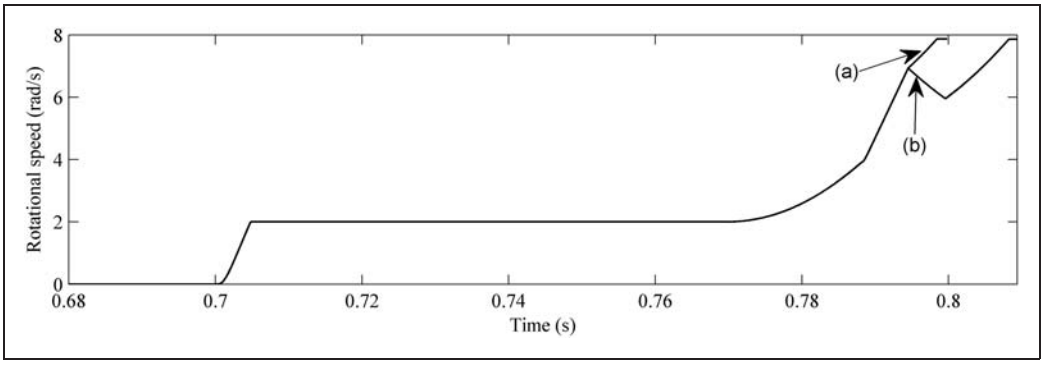

Figure 8. Sleeve displacement for both positive (a) and negative (b) chamfer flank contacts.

Simulations in Figure 9 present shift transient and synchronisation results for an engine speed at 400 rad/s. As a result of simulating at a higher speed, the speed synchronisation is increased from 60 ms in Figure 6(b) to 95 ms in Figure 9(b). The influence on ring unblocking and indexing during engagement is less significant with only a marginal variation in the duration of these processes. However, there is a noticeable reduction in the vibration resulting from synchroniser engagement in the powertrain. In comparison to Figure 6(a), Figure 9(a) shows a reduction in transient vibration in the post-synchronisation states of the powertrain. This change in initial speed also influences gear shift during the inertia phase and post-shift powertrain response. During the inertia phase, the severity of the vibration is reduced, and post-shift transients demonstrate a reduction in vibration amplitude of the 6 Hz mode beyond 1.4 s. This is attributed to both the reduced vibration in the inertia phase and increased damping in clutches.

Impact of shift timing

The impact of timing the synchroniser engagement with actuation of the clutches is studied through delaying the initiation of synchroniser engagement by 200 ms, thereby initiating synchronisation during shift preparation in the clutches. Initial conditions are otherwise consistent with those described at the beginning of 'Numerical simulations'. Clutch pressure profiles in Figure 5 suggest that CL1 pressure and hence maximum static friction is at a minimum from 1 to 1.1 s prior to the commencement of shifting. As shown in Figure 10, while synchroniser engagement and shifting proceeds very similarly to previous results, the reduced CL1 friction torque interacts with the synchroniser

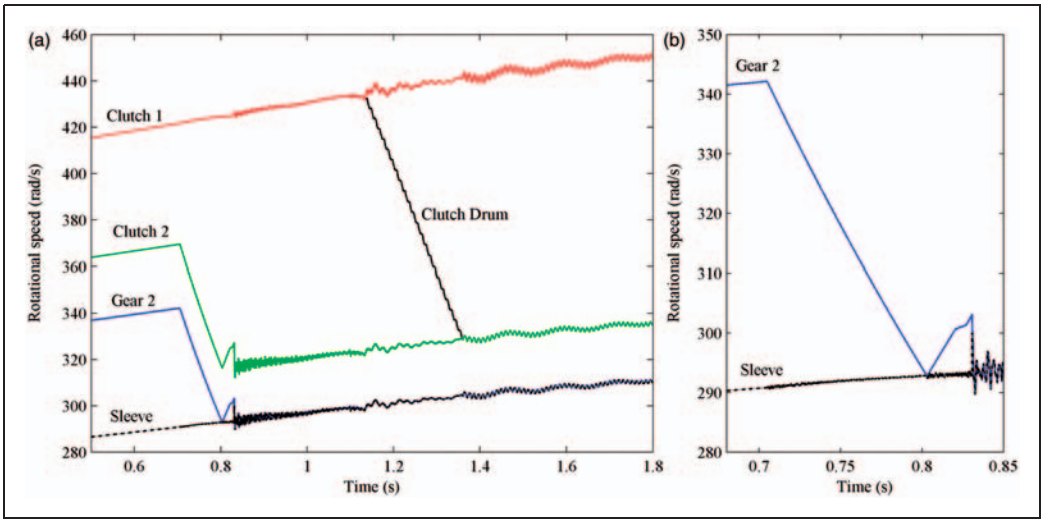

Figure 9. Simulation results for an initial engine speed of 400 rad/s (λ): (a) synchroniser engagement and shift transient for complete shift and (b) synchroniser engagement.

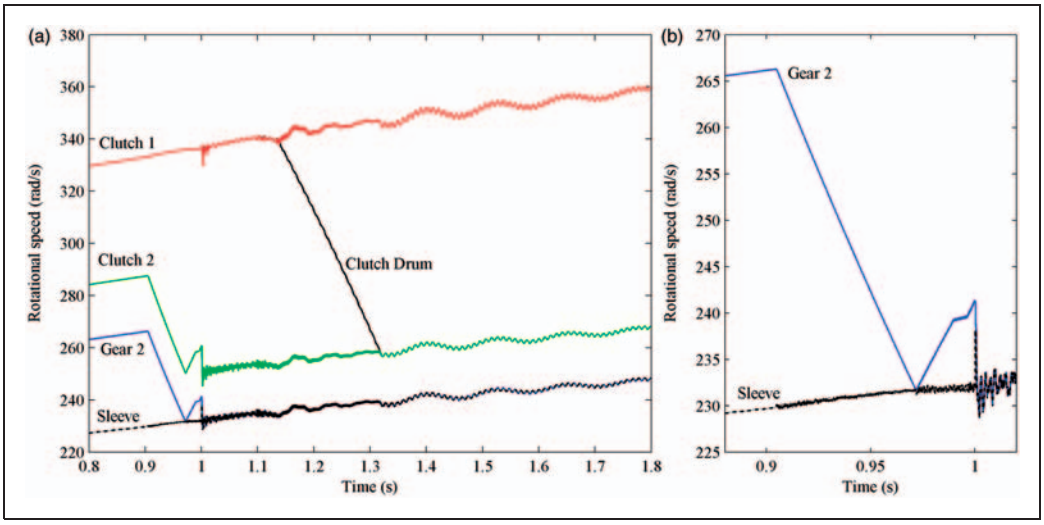

Figure 10. Simulation results for alternative synchroniser engagement timing: (a) synchroniser engagement and shift transient for complete shift and (b) synchroniser engagement.

lock-up and a brief period of stick-slip is initiated between CL1 and the clutch drum at a time of approximately 1 s, resulting in increased torque hole at the beginning of shifting and reducing the overall shift quality.

Conclusion

This article presented a comprehensive model of a DCT-equipped powertrain for the transient study of synchroniser engagement and gear-shift dynamics. The powertrain model was built as a multi-body dynamic model of the major powertrain components with provision for synchroniser engagement and clutch-to-clutch shifting. System states were defined by the combination of different synchroniser and clutch engagement. The model was then used to conduct shift transient studies of the powertrain for the combination of both synchroniser mechanism engagement and gear shift for the evaluation of system response to both transient events.

Simulations were then conducted to study the impact of different variables on the duration and quality of both synchronisation and gear shift. Consideration of chamfer alignment demonstrates that the dependency on contact flank results in variation of the duration

of synchroniser engagement. Additionally, the speed-matching phase of synchronisation is highly dependent on the vehicle speed, as is the inertia phase of gear shift. However, both these factors of chamfer alignment and vehicle speed have limited impact on the overall shift quality. The final consideration was placed on the timing of synchroniser engagement prior to gear shift. The results demonstrate that the delay of synchroniser engagement such that it overlaps with shift preparation in clutches can lead to a reduction in shift quality. This is a consequence of the impulse generated in the synchroniser at the completion of engagement interacting with the lower static friction limit in CL1 as shift preparation is performed.

Funding

Financial support for this research was provided by the Ministry of Science and Technology, China, through grant 2011DFB70060.

Acknowledgements

The support of Beijing Electric Vehicles is gratefully acknowledged.

References

1. Goetz M. *Integrated powertrain control for twin clutch transmissions*. PhD Thesis, University of Leeds, UK, 2005.
2. Kulkarni M, Shim T and Zhang Y. Shift dynamics and control of dual-clutch transmissions. *Mech Mach Theory* 2007; 42(2): 168–182.
3. Liu Y, Qin D and Jiang H. A systematic model for dynamics and control of dual clutch transmissions. *ASME J Mech Des* 2010; 131(6): paper no. 061012.
4. Goetz M, Levesley M and Crolla D. Dynamics and control of gearshifts on twin-clutch transmission. *Proc IMechE Part D: J Automob Eng* 2005; 219(8): 951–963.
5. Goetz M, Levesley M and Crolla D. Dynamic modelling of a twin clutch transmission for controller design. *Mater Sci Forum* 2003; 440–441: 253–261.
6. Goetz M, Levesley M and Crolla D. A gearshift controller for twin clutch transmissions. *VDI Ber* 2003; 1786: 381–400.
7. Xuexun G, Chang F, Jun Y, et al. Modeling and simulation research of dual clutch transmission based on fuzzy logic control. SAE paper 2007-01-3754, 2007.
8. Cheng X and Wang, Y. The intelligent down-shift control for wet dual clutch transmission. In: *2011 International conference on mechatronic science, electrical engineering and computer*, Beihua University, Jilin, China, 12–22 August, 2011, pp.189–192.
9. Kim J, Cho K and Choi SB. Gear shift control of dual clutch transmissions with a torque rate limitation trajectory. In: *2011 American control conference*, San Francisco, CA, 29 June–1 July 2011, pp.3338–3343.
10. Walker PD, Zhang N and Tamba R. Control of gear shifts in dual clutch transmission powertrains. *Mech Syst Signal Process* 2011; 26(6): 1923–1936.
11. Galvagno E, Velardocchia M and Vigliani A. Dynamic and kinematic model of a dual clutch transmission. *Mech Mach Theory* 2011; 46(6): 794–805.
12. Liu Y and Tseng C. Simulation and analysis of synchronisation and engagement on manual transmission gearbox. *Int J Veh Des* 2007; 43(1–4): 200–220.
13. Hoshino H. Analysis on synchronisation mechanism of transmission. SAE paper 1999-01-0734, 1999.
14. Walker PD and Zhang N. Parameter study of synchroniser mechanisms applied to dual clutch transmissions. *Int J Powertrains* 2011; 1(2): 198–220.
15. Socin RJ and Walters LK. Manual transmission synchronizers. SAE paper 680008, 1968.
16. De la Cruz M, Theodossiades S and Rahnjeat H. An investigation of manual transmission drive rattle. *Proc IMechE Part K: J Multi-body Dyn* 2009; 224(2): 167–181.
17. Fredriksson J and Karlsson J. Cylinder-by-cylinder engine models vs. mean value engine models for use in powertrain control applications. SAE paper 1999-01-0906, 1999.
18. Vasca F, Iannelli I and Senatore A. Transmissibility assessment for automotive dry-clutch engagement. *IEEE/ASME T Mech* 2011; 16(3): 564–573.
19. Crowther A, Zhang N and Liu DK. Analysis and simulation of clutch engagement judder and stick-slip in automotive powertrain systems. *Proc IMechE Part D: J Automob Eng* 2004; 218(12): 1427–1446.
20. Paffoni B, Progri R and Gras R. The hydrodynamic phase of gearbox synchromesh operation: the influence of radial and circumferential grooves. *Proc IMechE Part J: J Eng Tribol* 1997; 211(2): 107–116.
21. Walker PD, Zhang N and Tamba R. Dynamics and simulations of shifting in a dual clutch transmission. In *6th Australasian congress on applied mechanics,* Institute of Engineers Australia, Perth, Australia, 12–15 December 2010, paper no. ACAM-1110.

Appendix 1

Notation

A_V	frontal vehicle area
b	half-cone generatrix
C	damping elements (refer to Table 3 for subscripts)
C_D	drag coefficient
C_T	rolling resistance of the tyre
f_C	cone clutch friction coefficient
$f_{C,S}$	cone clutch static friction coefficient
F	synchroniser sleeve force
F_A	force from the hydraulic load on the clutch
h	cone clutch separation
I	inertia elements (refer to Table 3 in Appendix 2 for subscripts)
K	stiffness elements (refer to Table 3 in Appendix 2 for subscripts)
M_V	vehicle mass
n	number of friction surfaces

r_I	inside clutch radius	X_0	minimum primary clutch contact displacement
r_O	outside clutch radius		
R_C	cone clutch mean radius	X_S	synchroniser sleeve displacement
R_I	indexing chamfer radius	X_{S0}	minimum synchroniser contact displacement
R_W	wheel radius		
T_{avg}	average torque in an engaged clutch	α	cone clutch angle
T_C	cone clutch torque	β	chamfer angle
T_{C_1}	CL1 torque	$\dot{\theta}_{SYN}$	synchroniser slip speed,
T_{C_2}	CL2 torque	$\theta, \dot{\theta}, \ddot{\theta}$	rotational displacement, velocity and acceleration of elements
$T_{C,S}$	cone clutch static friction torque		
T_E	engine torque	λ	chamfer contact flank
T_{S1}	S1 torque	μ	lubricant viscosity
T_{S2}	S2 torque	μ_D	dynamic friction coefficient of primary clutches
T_V	vehicle torque		
V	linear velocity of the vehicle	μ_I	chamfer friction coefficient
$\dot{x}$	synchroniser sleeve	μ_S	static friction coefficient of primary clutches
X	primary clutch piston displacement	ρ_{air}	air density
		φ	road grade

Appendix 2

Powertrain system properties

Table 2. Transmission ratios.

Transmission ratio	Name	Value	Transmission ratio	Name	Value
γ_1	Third gear	1.45	γ_3	Final drive 1	3.14
γ_2	Fourth gear	1.08	γ_4	Final drive 2	3.14

Table 3. Powertrain properties.

Inertia element	Name	Value (kg-m^2)	Stiffness element	Value (Nm/rad)
I_1	Engine	0.4	K_1	94,250
I_2	Flywheel	0.2	K_2	200,000
I_3	Clutch drum	0.2	K_3	210,000
I_4	CL1	0.0072	K_4	560,000
I_{5A}	Gear 1	0.0145	K_5	870,000
I_{5B}	Pinion 1	0.0025	K_6	470,000
I_6	S1	0.005	K_7	488,000
I_7	CL2	0.0125	K_8, K_{10}	49,000
I_{8A}	Gear 2	0.0094	K_9, K_{11}	20,000
I_{8B}	Pinion 2	0.0013	Damping element	Value (Nms/rad)
I_9	S2	0.005	C_1	2
I_{10A}	Final drive 1	0.0028	C_2	0.049
I_{10B}	Final drive 2	0.00094	C_3	0.0044
I_{10C}	Final drive 3	0.16	C_4	0.0052
I_{11}	Differential	1	C_5	0.01
I_{12}	Wheel hub 1	1.2	C_6	0.023
I_{13}	Tyre and half vehicle 1	67.56	C_7	10
I_{14}	Wheel hub 2	1.2	C_8	0.1
I_{15}	Tyre and half vehicle 2	67.56	C_9, C_{10}	40

CL1: clutch 1; S1: synchroniser 1; CL2: clutch 2; and S1: synchroniser 1.